Magnetic billiards on a torus with a uniform field in a disk

Albert Šilvans, s3400166

June 17, 2023

Contents

List of Figures

List of Tables

1 Introduction

Our main point of interest is the long term dynamics of a particle in the presence of a magnetic field, specifically, we consider the case of a magnetic billiard. Similar work has been done in [KS17], where the focus was scattering for finitely many *bumps*, and [Gas21] where many non-trivial periodic orbits were found for "inverted" bumps, that is, the magnetic field only vanished on the bumps. We follow in the same vein but consider infinitely many bumps in a lattice, and describe the dynamics using various methods.

1.1 The electromagnetic field Hamiltonian

Classically, the trajectory of a particle in $\mathbb{R}^3$ in the presence of a magnetic field is described by the solutions of the Hamiltonian:

$$H(q,p) = \frac{1}{2m}\left\|p - \frac{e}{c}A(q)\right\|^2 + U(q)$$

where $q = (q_1, q_2, q_3)$ and $p = (p_1, p_2, p_3)$ are the position and momentum, $m, e, c > 0$ are physical parameters, $U : \mathbb{R}^3 \to \mathbb{R}$ is a potential function, and $A : \mathbb{R}^3 \to \mathbb{R}^3$ is a magnetic vector field. For our purposes, we can absorb the physical parameters into the momentum variable and the vector field, effectively, we set $m = e = c = 1$, and we focus on the case $U(q) = 0$ for simplicity. Hence, we study solutions of

$$H(q,p) = \frac{1}{2}\left\|p - A(q)\right\|^2, \tag{1}$$

where A is still to be prescribed. The equations of motion are given by the system:

$$\dot{q}_i = \frac{\partial H(q,p)}{\partial p_i} = p_i - A_i(q) \tag{2a}$$

$$\dot{p}_i = -\frac{\partial H(q,p)}{\partial q_i} = -\sum_{k=1}^{3}\Big(p_i - A_i(q)\Big)\frac{\partial A_k}{\partial q_i} \tag{2b}$$

where $A_k(q)$ denotes the k-th component of A. To further limit the breadth of study, we consider some restrictions on A. First, we consider only motion in the (q_1, q_2)-plane, so only trajectories that have initial condition $q = (q_1, q_2, 0)$ and $p = (p_1, p_2, 0)$, and that satisfy $q_3(t) = p_3(t) = 0$ for all $t \geq 0$. For this to be satisfied, we need that $\dot{q}_3 = p_3 - A_3(q) = 0$, which also implies that $A_3(q) = 0$ for all $t \geq 0$. We also need $\dot{p}_3 = 0$, which means that

$$\Big(p_1 - A_1(q)\Big)\frac{\partial A_1}{\partial q_3} + \Big(p_2 - A_2(q)\Big)\frac{\partial A_2}{\partial q_3} = 0.$$

This is a first order differential equation in 2 unknown functions, which is not sufficient to determine a unique solution. An example of a family that satisfies the above:

$$A(q_1, q_2) = (A_1(q_1, q_2), A_2(q_1, q_2), 0).$$

The second criteria we want: A is 1-periodic in q_1 and q_2, so

$$A(q_1 + 1, q_2 + 1, q_3) = A(q_1, q_2, q_3)$$

In particular, we will later use the vector field $A(q) = (-\varepsilon(q_2 \bmod 1), 0, 0)\mathbb{1}_S$ where $\varepsilon > 0$ and $\mathbb{1}_S$ is the indicator function on $S \subseteq \mathbb{R}^3$ which is a union of cylinders:

$$S = \bigcup_{n,m\in\mathbb{Z}} \left\{ q \in \mathbb{R}^3 : \left(q_1 - n - \frac{1}{2}\right)^2 + \left(q_2 - m - \frac{1}{2}\right)^2 \leq R^2 \right\},$$

where $R \in (0, 1/2)$. Writing out the final form of the Hamiltonian we consider:

$$H(q,p) = \frac{1}{2}\left(p_1^2 + p_2^2\right) + \varepsilon q_2 \left(p_1 + \frac{\varepsilon q_2}{2}\right)\mathbb{1}_S = H_0(q,p) + \varepsilon H_1(q,p,\varepsilon) \tag{3}$$

where we ignore q_3 completely. We define H_0 and H_1 for later use, H_0 denotes the unperturbed Hamiltonian and H_1 the perturbation.

We immediately notice that (3) is discontinuous along the boundary ∂S of S, and this becomes an issue when considering trajectories that pass ∂S tangentially. For some values of $\varepsilon > 0$ we will find that the solution to (3) can be non-unique. We argue however that the dynamics of these solutions is not important, since ∂S is a set of measure zero. Throughout the paper though we assume that if a trajectory does pass ∂S tangentially, then it does not enter S.

We also notice that we can express (3) as a Hamiltonian on the torus $\mathbb{T}^2 = \mathbb{R}^2\backslash\mathbb{Z}^2$ via the usual quotient map which will be convenient for some proofs later. To fully comprehend the dynamics of (3) both in $\mathbb{R}^2$ and $\mathbb{T}^2$ we first discuss the dynamics of each piece separately. That is, we refresh our memory on linear motion in the plane, rotations in a torus, and motion in a uniform magnetic field in the plane.

1.2 Linear motion and rotations on the torus

Here we discuss solutions of the Hamiltonian $H : \mathbb{R}^2 \to \mathbb{R}^2$ with $H(q,p) = \|p\|^2/2$ in the plane and in the torus. The equations of motion can be computed readily from the Hamiltonian system, they are:

$$V_1(t) = (q_1(t), q_2(t)), \qquad q_1(t) = p_1 t + q_1(0), \qquad q_2(t) = p_2 t + q_2(0) \tag{4}$$

where $p_1, p_2 \in \mathbb{R}$ are constants. We understand this motion well, it is just straight lines in the plane.

The situation becomes more interesting when we consider the induced motion on the quotient space $\mathbb{T}^2 = \mathbb{R}^2\backslash\mathbb{Z}^2$ via the quotient $P : \mathbb{R}^2 \to \mathbb{T}^2$ with $P(q_1, q_2) = (q_1 \bmod 1, q_2 \bmod 1) = [q_1, q_2]$, where the bracket indicates the equivalence class of the point (q_1, q_2). The equations become:

$$\hat{V}_1(t) = P \circ V_1(t) = [q_1(t), q_2(t)] = t[p_1, p_2] + [q_1(0), q_2(0)], \tag{5}$$

so the trajectory that was a line in the plane now wraps around the torus. It is now important to understand how the ratio of p_1 to p_2 influences the dynamics.

Definition 1. Let $p_1, p_2 \in \mathbb{R}$, we say p_1, p_2 are *rationally dependent* if there exist $n, m \in \mathbb{Z}$ such that $p_1 n + p_2 m = 0$.

Two numbers are then called *rationally independent* if there does not exist a pair of integers satisfying the equation. This definition helps us formulate the following well-known result.

Proposition 1. Consider the trajectory $\hat{V}_1$ of (5) in the torus.

1. If p_1 and p_2 are rationally dependent, then $\hat{V}_1$ is a periodic solution, and its orbit $\hat{V}_1([0,\infty))$ is a closed curve on the torus,
2. If p_1 and p_2 are rationally independent, then $\hat{V}_1([0,\infty))$ is dense in the torus.

Another result that can be mentioned here but will not be important in our discussion is that due to Proposition 1 the set of periodic orbits is dense in phase space.

1.3 Uniform magnetic vector field in the plane

We focus now on (1) and take $A(q) = (-\varepsilon q_2, 0, 0)$ and $\varepsilon > 0$ as used for (3), except, we do not include the indicator $\mathbb{1}_S$. This gives the Hamiltonian for the motion of a particle in the (q_1, q_2)-plane in the presence of a vector field in the plane.

$$H(q,p) = \frac{1}{2}(p_1 + \varepsilon q_2)^2 + \frac{1}{2}p_2^2, \tag{6}$$

From H, we find Hamilton's equations:

$$\begin{aligned} \frac{dq_1}{dt} &= 2(p_1 + \varepsilon q_2) & \frac{dq_2}{dt} &= 2p_2 \\ \frac{dp_1}{dt} &= 0 & \frac{dp_2}{dt} &= -2\varepsilon(p_1 + \varepsilon q_2). \end{aligned}$$

And we can find the equations of motion: $X_2(t) = (q_1(t), q_2(t))$ with

$$q_1(t) = \alpha_1 - R\cos(\varepsilon t + \varphi), \qquad q_2(t) = \alpha_2 + R\sin(\varepsilon t + \varphi)$$

where $\alpha_1, \alpha_2, R, \varphi$ are integration constants. These can be computed explicitly:

$$\begin{aligned} \alpha_1 &= q_1(0) + \frac{p_2(0)}{\varepsilon} & R &= \frac{1}{\varepsilon}\|X_2'(t)\| \\ \alpha_2 &= q_2(0) - \frac{p_1(0)}{\varepsilon} & \varphi &= \operatorname{arctan2}\left(p_1(0), p_2(0)\right) \end{aligned}$$

where arctan2 behaves like arctan with the added benefit that it correctly determines the quadrant of the angle. From the equations of motion, we see that the orbits are circles which we call *Larmor* circles. The *Larmor* radii R and centers (α_1, α_2) of the circles are determined uniquely by the initial conditions of the particle as we can see above.

1.4 interplay of linear motion and magnetic fields

In the previous sections we determined the local behavior of the system (3), that is, outside the magnetic disks the particle travels along straight lines, and in the

magnetic disks it travels along arc of circles. Respectively, on a torus, there is winding around the torus, and circular arcs. What is interesting to study now is the interplay of linear motion and deflection. Specifically, considered separately, the two modes of motion are easy to predict, meanwhile, when considered together: a particle leaving a magnetic disk may enter one of the neighboring ones, or given the right conditions, it can evade the disks for a "long" time.

2 Weak magnetic field and KAM theory

We begin by recalling Kolmogorov-Arnold-Moser (KAM) theory, state one of the main KAM theorems, and briefly outline the main points of the theory before delving into its application. We refer the reader to [Kna18] and [Ser22] for a more detailed account. We strongly recommend [Pö82] for reference, as it is the version of KAM we use here.

KAM theory is a method for studying perturbations of integrable Hamiltonian systems. Its origins lie in Celestial and Hamiltonian mechanics, where it was used to study the orbits of planets. Hamiltonian mechanics is a strong tool for modeling and studying systems, however it is strongest for conservative systems. Naturally, we find in practice many non-conservative systems, or conservative ones that are too complicated in full, in which case a smaller subsystem is modeled and the rest is viewed as a perturbation. We are interested in the second scenario, we denote by $H^0(q,p)$ an integrable Hamiltonian and by $H^1(q,p,\varepsilon)$ a perturbation.

Focusing on the integrable case, it is known by the Liouville-Arnold theorem that there exist *action-angle* coordinates so that $H^0 := H^0(p)$ can be expressed in terms of the action variable only. The equations of motion in action-angle coordinates are given by:

$$\dot{q} = \omega, \qquad \dot{p} = 0,$$

where $\omega = \partial_p H^0(p)$ and $\partial_p H^0 : I \to \Omega$ is the so-called *frequency map*. In these action-angle coordinates, the phase space becomes $\mathbb{T}^n \times I$ where $I \subseteq \mathbb{R}^n$ and the dynamics of the system are completely expressed as rotations on the torus. Specifically, phase space is foliated into a family of invariant tori $\mathbb{T}^n \times \{p\}$ for each $p \in I \subseteq \mathbb{R}^n$. We consider only integrable Hamiltonians with a *non-degenerate* frequency map, that is, $\det \partial_p^2 H^0 \neq 0$. Now, KAM deals with Hamiltonians of the form

$$H(q,p) = H^0(p) + \varepsilon H^1(q,p),$$

where $1 \gg \varepsilon > 0$ is considered small, H^0 is the integrable part and H^1 is the perturbation. We assume that H is 2π-periodic in each component of q. What KAM theory ensures is that under the correct conditions, a "large" subset $\Omega_{\gamma,\tau} \subseteq \Omega$, $\gamma, \tau > 0$ of invariant tori of $H^0(p)$ are preserved, though possibly deformed, under the perturbation H^1. The set $\Omega_{\gamma,\tau}$ is given by:

$$\Omega_{\gamma,\tau} = \bigcap_{\substack{k \in \mathbb{Z} \\ k \neq 0}} \left\{ \omega \in \Omega : |\omega \cdot k| \geq \gamma |k|^{-\tau} \right\}. \tag{7}$$

The condition for $\Omega_{\gamma,\tau}$ is called the *small divisor condition*. It can be shown for $\tau > n-1$ that for almost all $x \in \mathbb{R}^n$ there exists a $\gamma > 0$ such that $x \in \Omega_{\gamma,\tau}$,

so in particular, we can find $\gamma > 0$ so that a point $\omega \in \Omega$ satisfies $x \in \Omega_{\gamma,\tau}$. We finally consider the *Cantor* set

$$\hat{\Omega}_{\gamma,\tau} = \Omega_{\gamma,\tau} \cap \{\omega \in \Omega : d(\omega, \partial\Omega) \geq \gamma\},$$

that is, we remove points in $\Omega_{\gamma,\tau}$ that have distance less than γ from the boundary of Ω. It can be shown $\Omega \backslash \bigcup_{\gamma>0} \hat{\Omega}_{\gamma,\tau}$ is a set of measure zero, so the measure of Ω_γ becomes large for small γ ,justifying the term "large". We can now give the KAM theorem as stated in [Pö82].

Theorem 1. Let the integrable Hamiltonian $H^0 : \mathbb{T}^n \times I \to \mathbb{R}$ be real analytic and non-degenerate, such that the frequency map $\partial_p H^0 : I \to \Omega$ is a diffeomorphism and let the perturbed Hamiltonian $H = H^0 + \varepsilon H^1$ be of class $C^{\alpha\lambda+\lambda+\tau}$ with $\lambda > \tau + 1 > n$ and $\alpha > 1$. Then there exists a positive γ-independent δ such that for $|\varepsilon| < \gamma^2\delta$ with γ sufficiently small, there exists a diffeomorphism

$$\mathcal{T} : \mathbb{T}^n \times \Omega \to \mathbb{T}^n \times I,$$

which on $\mathbb{T}^n \times \hat{\Omega}_{\gamma,\tau}$ transforms the equations of motion of H into

$$\dot{\theta} = \omega, \qquad \dot{\omega} = 0.$$

The map $\mathcal{T}$ is of class C^α for non-integer α and close to the inverse of the frequency map; its Jacobian determinant is uniformly bounded from above and below. In addition, if H is of class $C^{\beta\lambda+\lambda+\tau}$ with $\alpha \leq \beta \leq \infty$, then one can modify $\mathcal{T}$ outside $\mathbb{T}^n \times \hat{\Omega}_{\gamma,\tau}$ so that $\mathcal{T}$ is of class C^β for noninteger β.

So, for $\omega \in \hat{\Omega}_{\gamma,\tau}$, we parametrize an invariant torus via the map $\theta \mapsto \mathcal{T}(\theta, \omega)$. There are a few theorems in use now that are titled the *KAM theorem*, and they differ mainly whether they discuss analytic or smooth perturbations. It is easier to find sources discussing the analytic versions, since they provide stronger results about the invariant torii. Having said this, we use the C^r version because it is easier to construct smooth approximations of discontinuous functions as opposed to analytically approximating them.

2.1 Approximating locally L^1 functions for KAM

The Hamiltonian (3) we wish to study is discontinuous, which by itself is not suitable for the KAM theorem. We can, however, smoothly approximate the Hamiltonian by using *mollifiers*. The *standard mollifier* $\varphi : \mathbb{R}^n \to \mathbb{R}$ is the following function:

$$\varphi(x) = \begin{cases} c \exp\left(\frac{1}{|x|^2-1}\right), & |x| < 1 \\ 0, & |x| \geq 1, \end{cases}$$

where $c > 0$ is a scaling factor chosen so that the integral of φ over $\mathbb{R}^n$ is 1. Also, φ is commonly called a *bump* function, since its support is compact. For $\varepsilon > 0$, let

$$\varphi_\varepsilon(x) = \frac{1}{\varepsilon^n} \varphi\left(\frac{x}{\varepsilon}\right),$$

this function has the following properties:

$$\varphi_\varepsilon \in C_c^\infty(\mathbb{R}^n), \quad \varphi \geq 0, \quad \int_{\mathbb{R}^n} \varphi = 1, \quad \operatorname{supp}(\varphi_\varepsilon) \subset B_\varepsilon(0) = \{x \in \mathbb{R}^n : |x| < \varepsilon\},$$

that is, the function φ_ε is smooth in $\mathbb{R}^n$ with compact support, it is positive, its integral is 1, and the support of φ_ε is fully contained in the unit ball of radius $\varepsilon > 0$ centered at the origin.

Let $f \in L^1_{\text{loc}}(X)$ be a locally integrable function in $X \subseteq \mathbb{R}^n$. The *mollification* of f is defined as the convolution of f with φ_ε, that is, $\varphi_\varepsilon * f : X_\varepsilon \to \mathbb{R}$ where $X_\varepsilon = \{x \in X : d(x, \partial X) > \varepsilon\}$. Explicitly,

$$f_\varepsilon(x) = \big(\varphi_\varepsilon * f\big)(x) = \int_X \varphi_\varepsilon(x-y) f(y) dy = \int_{B_\varepsilon(0)} \varphi_\varepsilon(y) f(x-y) dy, \quad x \in X_\varepsilon$$

Some properties that the mollification f_ε has are summarized here:

Theorem 2. Let $f \in L^1_{\text{loc}}(X)$. Then the mollification f_ε has the following properties:

1. $f_\varepsilon \in C^\infty(X_\varepsilon)$,
2. $f_\varepsilon \to f$ almost everywhere as $\varepsilon \to 0$,
3. if f is continuous on X, then $f_\varepsilon \to f$ as $\varepsilon \to 0$ uniformly on compact subsebts of X,
4. if $1 \leq p < \infty$ and $f \in L^p_{\text{loc}}(X)$, then $f_\varepsilon \to f$ as $\varepsilon \to 0$ in $L^p_{\text{loc}}(X)$

Proof. The proof of this theorem can be found in Appendix C of [Eva98] ■

What we gain from Theorem 2 is not only a smooth approximation of our discontinuous Hamiltonian but an approximation that can be made arbitrarily precise almost everywhere. Of course, the points which cannot be approximated accurately are concentrated at the boundary of each disk, where the discontinuities lie. Despite this, it is reasonable to assume that for sufficiently small values of ε, the flow of the equations of motion provided by the mollified Hamiltonian approximate very well the flow of the disconitinuous one.

In fig. 1 we numerically solve the system and observe some interesting relations. First, we see in each figure the trajectory for $b = 0.1$ appears as a smear near the origin, this is likely because b is large enough for the deflection in each disk to be significant. For the other values of b, we see the trajectories follow a circular arc, and for smaller b the radius of the respective circular arc is larger. In the limit $b \to 0$, the trajectories will straighten out, since the magnetic field vanishes. This motivates the use of KAM, specifically, considering the Hamiltonian $H_0(q,p) = \|p\|^2/2$ and introducing the bumps as a perturbation when $b \approx 0$.

Alternatively, since the trajectories follow circular arcs, this suggests we can consider the motion as a perturbation of a different Hamiltonian. Specifically, we conjecture that we should start with a non-zero magnetic Hamiltonian with vector potential $A = (-\hat{b}q_2, 0, 0)$ in the plane with strength $\hat{b}$ and perturb it to the case with the bumps of strength b.

We first reason heuristically to see that this idea is valid. Comparing the trajectories for $b = 0.01$ and 0.001 in fig. 1a and 1b, we see that the radius

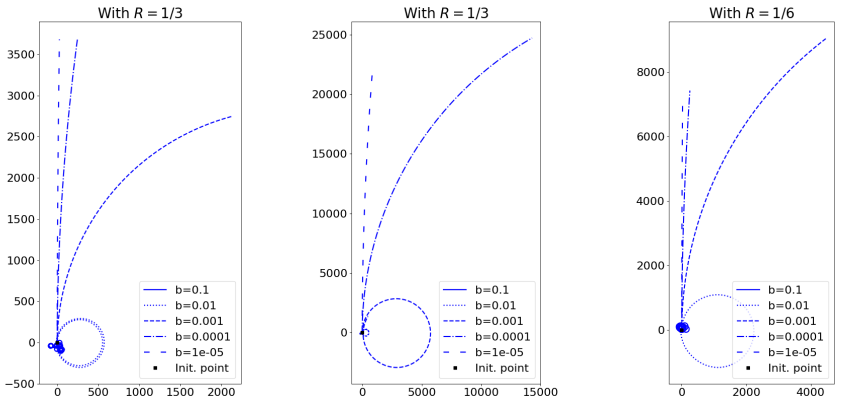

(a) (b) (c)

Figure 1: Each plot shows 5 trajectories for varying $b = 10^{-1}, \ldots, 10^{-5}$. In fig. 1a and fig. 1b the init. cond. and params. are the same $X \approx (0.38, 0.81)$ and $V \approx (0, 1)$, and $R = 1/3$, only the duration of the simulation differs. In fig. 1c, V is the same, $X \approx (0.44, 0.65)$ and $R = 1/6$.

of the trajectory is ≈ 250 and ≈ 2500, respectively. If we assume this is the value of the Larmor radius $\hat{L}$ in each case, then we see $\hat{L} \propto 1/b$ or $\hat{b} \propto b$. Now, comparing the trajectories for $b = 0.01$ in fig. 1a and 1c, we see halving the radius R of the magnetic bumps roughly quadruples the radius $\hat{L}$ from 250 to 1000, that is, $\hat{L} \propto 1/R^2$, and the strength then relates as $\hat{b} \propto R^2 b$. The task then is to determine $C \in \mathbb{R}$ such that $\hat{b} = CR^2 b$.

We can reason another way. W.l.o.g. consider $[0, 1]^2$, we would like the uniform field with strength $\hat{b}$ to have the similar deflection of trajectories as the field with strength b in the disk with radius R. How much a trajectory is deflected depends on the flux of the field, so if we equate the fluxes $\Phi_B = \Phi_{\hat{B}}$, we can compute the required strength $\hat{b}$ for $\hat{B}$. Recall, that the magnetic flux is given by:

$$\Phi_B = \iint_S \mathbf{B} \cdot dA = \iint_S \nabla \times \mathbf{A} \cdot dA,$$

so it is the integral of the vector field $\mathbf{B}$ through the surface S. Computing the flux for a uniform field in S, we get

$$\Phi_{\mathbf{B}} = \iint_S \mathbf{B} \cdot dA = \iint_S (0, 0, b) \cdot (0, 0, 1) dA = bA(S),$$

where $A(S)$ denotes the area of the surface. In our case, $\Phi_{\hat{\mathbf{B}}} = \Phi_{\mathbf{B}}$ implies $\hat{b} = \pi R^2 b$, which is about what we expected. We collect and process some data that corroborates this finding in a later section.

2.2 Perturbations of linear motion

Recall, that a particle in the plane moves along Larmor circles when in the presence of a uniform magnetic field, with strength b, orthogonal to the plane

of motion. The Larmor radius R depends inversely with respect to the field strength, $Rb \propto 1$, that is, a weaker the field strength corresponds to a larger Larmor radius. So, as $b \to 0$, we expect $R \to \infty$, which means that locally the trajectory approaches linear motion in the plane. This intuition is coroborated when considering the Hamiltonian (6) and setting $\varepsilon = 0$. Hence, it is natural to consider the Hamiltonian $H_0(q,p) = \|p\|^2/2$ and study perturbations of it via KAM

We readily see that H_0 is real analytic, it is already in action-angle coordinates from which we can deduce it is non-degenerate $\det \partial_p^2 H_0 = 1 \neq 0$, and the frequency map $\partial_p H_0(p) = p$ is a diffeomorphism. Now, recall the Hamiltonian (3) with $A(q) = (-b(q_2 \bmod 1), 0, 0)\mathbb{1}_S$ where S is the set of disks in the plane, and attempt to isolate the perturbation term from the linear motion.

$$\begin{aligned} H(q,p) = \frac{1}{2}\|p - A(q)\|^2 &= \frac{1}{2}\left(p_1 + b(q_2 \bmod 1)\mathbb{1}_S\right)^2 + \frac{1}{2}p_2^2 \\ &= \frac{1}{2}\left(p_1^2 + 2p_1 b(q_2 \bmod 1)\mathbb{1}_S + b^2(q_2^2 \bmod 1)\mathbb{1}_S^2\right) + \frac{1}{2}p_2^2 \\ &= \frac{\|p\|^2}{2} + b\frac{(q_2 \bmod 1)}{2}\left(2p_1\mathbb{1}_S + b(q_2 \bmod 1)\mathbb{1}_S^2\right) \\ &= \frac{\|p\|^2}{2} + b\frac{(q_2 \bmod 1)}{2}\left(2p_1 + b(q_2 \bmod 1)\right)\mathbb{1}_S \\ &= H_0(q,p) + bH_1(q,p,b) \end{aligned}$$

where we used $\mathbb{1}_S^2 = \mathbb{1}_S$ for indicator functions. We see now explicitly the perturbation H_1. As previously discussed, H_1 is discontinuous on $\mathbb{R}^2$, and to apply KAM, we need to mollify H_1. Hence, consider the standard mollifier $\varphi_\varepsilon(q,p) = \varphi_\varepsilon(x) : \mathbb{R}^2 \to \mathbb{R}$ and let $\hat{H}_1 = \varphi_\varepsilon * H_1$, notice that we do not mollify with respect to the parameter b.

Now, $\hat{H} = H_0 + b\hat{H}_1$. Recalling Theorem 1 we need $\hat{H}$ to be at least of class $C^{\alpha\lambda+\lambda+\tau}$ with $\lambda > \tau + 1 > n = 2$ and $\alpha > 1$. Since $\hat{H}$ is smooth, we can choose any $\tau > 1$, and Theorem 1 guarantees for sufficiently small $\gamma > 0$, there exists a $\delta > 0$ such that for field strengths b with $|b| < \gamma^2\delta$ we can preserve the invariant tori with frequencies in Ω_γ.

2.3 Perturbation of motion in a constant field

From fig. 1 we saw that instead of perturbing a linear Hamiltonian, we can try perturbing a Hamiltonian for a uniform magnetic field in the plane. If R is the radius of the magnetic disks, b the strength of the field, L the Larmor radius for b, and likewise for $\hat{L}$ and $\hat{b}$, we proposed a relation $\hat{b} = \pi R^2 b$.

To test the validity of the relation, we give two tests, the results of which can be found in fig. 2. In fig. 2a we generated data varying both R and b, and fit a general cubic of the form:

$$a_0 + a_1 R + a_2 b + a_3 R^2 + a_4 Rb + a_5 b^2 + a_6 R^3 + a_7 R^2 b + a_8 Rb^2 + a_9 b^3 = \hat{b} = 1/\hat{L},$$

using a least-squares method. In fig. 2b the same is done but first we fix $R = 1/3$ and then fit a line $a_0 + a_1 R^2 b$.

We generated the data as follows: for $1 \leq i \leq 50$ we sample values (R_i, b_i) uniformly in the range $[0.25, 0.45] \times [10^{-10}, 10^{-6}]$ (in the second test $R_i = 1/3$). For R_i, b_i we uniformly sample initial conditions X_{ij} with $1 \leq j \leq 20$. We fit a

circle to the trajectory of each X_{ij} and from these circles we extract the radius $\hat{L}_{ij}$. Finally, we take the average $\hat{L}_i = \sum_{j=1}^{20} \hat{L}_{ij}/20$.

To fit the circles we use the method of I. Coope which uses a change of coordinates to bring a non-linear least squares problem to the form of a linear problem. The set up and advantages of this method are discussed in [Coo93], and our use of it can be viewed at [??].

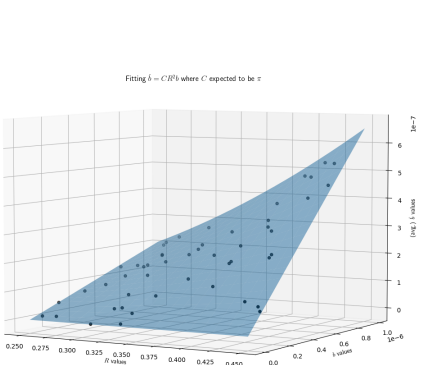

(a) Fitting a cubic surface

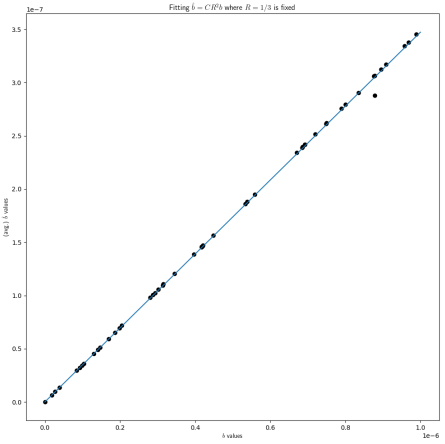

(b) Fitting a line

Figure 2: Fitting surfaces and lines to data to determine the parameter in our model.

The coefficients of the fitted cubic surface in fig. 2a come out to

$$a_0 \approx 6.7 \cdot 10^{-8}, \quad a_1 \approx -6.2 \cdot 10^{-7}, \quad a_2 \approx 6.7 \cdot 10^{-3},$$
$$a_3 \approx 1.9 \cdot 10^{-6}, \quad a_4 \approx -5.3 \cdot 10^{-2}, \quad a_5 \approx -1.9 \cdot 10^{+2},$$
$$a_6 \approx -1.8 \cdot 10^{-6}, \quad a_7 \approx 3.2, \quad a_8 \approx -6.6 \cdot 10^{+1},$$
$$a_9 \approx -3.0 \cdot 10^{-4},$$

the values of a_0 to a_4, a_6 and a_9 are negligible as expected, likewise $a_7 \approx \pi$. We notice that a_5 and a_8 are quite large but we reason that the contribution of their respective monomial term is still small, since both contain a factor of b^2 which has an order of magnitude at most 10^{-6}. The coefficients of the fitted line in fig. 2b are $a_0 \approx 4.4 \cdot 10^{10}$ and $a_1 \approx 3.12$, which can be explained in the same way. So, the relation $\hat{b} = \pi R^2 b$ seems valid, and this motivates perturbing a uniform magnetic field into the bump field

Overall, the results show that our assumptions are plausible, we approximately see π in the coefficient. The results are not as precise as desired but that can be due to randomly choosing the initial conditions for the trajectories. The circular trajectories correspond to invariant tori, and since not all tori are preserved under the perturbation, we expect that, chosen at random, some trajectories will not follow closely a circular path. Similarly, the chosen range for sampling R and b could be too large, though in tests we made that we omit here, we noticed that the relation holds more or less for a wider range of $[0.1, 0.45] \times [10^{-16}, 10^{-2}]$.

3 A step towards symbolic dynamics

Previously, we discussed the dynamics of (3) from the perspective of perturbation theory. Now, we attempt to extract some meaningful symbolic dynamics. We specify *meaningful* dynamics because we fail to do so via the standard approach: finding a markov partition and a conjugation to the shift map, instead we consider a reasonable map into a symbol space and judge the dynamics via the Lempel-Ziv complexity measure. What we find is two complementary methods to characterize the dynamics.

3.1 Constructing a Poincaré section

To simplify the notation, we consider motion in the torus $\mathbb{T} = [0,1]^2$, this way we need only refer to one disk $S = \{x \in \mathbb{T} : \|x - 1/2\| \leq R\}$. We recall the trajectories have two modes: linear outside the magnetic disk S, and along circular arcs within the disk. Consider two subsets $S_{\text{in}}, S_{\text{out}} \subset \mathbb{T} \times \mathbb{R}^2$ of phase space defined by:

$$S_{\text{in}} = \bigcup_{x \in \partial S} \{x\} \times \{v \in \mathbb{R}^2 : v \cdot (x - 1/2) < 0\}, \tag{8}$$

$$S_{\text{out}} = \bigcup_{x \in \partial S} \{x\} \times \{v \in \mathbb{R}^2 : v \cdot (x - 1/2) > 0\}, \tag{9}$$

so S_{in} is the part of phase space that lies on the boundary ∂S and has velocity vector pointing into S, while S_{out} points outward. Notice that we exclude velocities that are tangential to ∂S. We show now that both S_{in} and S_{out} are poincare sections of the full system.

Lemma 1. The flow of (3) induces a well-defined map $P_{\text{io}} : S_{\text{in}} \to S_{\text{out}}$.

Proof. Let $(x, v) \in S_{\text{in}}$, under the flow of (3) we know the Larmor circle C with initial conditions (x, v) intersects ∂S in x and that at x the circles are not tangential. Two circles intersecting at a point non-tangentially must intersect at a second point, so there exists $x \neq y \in \partial S \cap C$. By the flow of (3) there must also exist a velocity $w \in \mathbb{R}^2$ such that $w \cdot (x - 1/2) > 0$, that is $(y, w) \in S_{\text{out}}$. Hence we have $P_{\text{io}}(x, v) = (y, w)$. ∎

We can say more, there exists a line ℓ through the center a of the Larmor circle C and the center $(1/2, 1/2)$ of ∂S. The two circles are symmetric with respect to the reflection T with respect to ℓ. This means $Tx = y$, and $Tv = -w$. The following statement is more interesting.

Lemma 2. The flow of (3) induces a well-defined map $P_{\text{oi}} : S_{\text{out}} \to S_{\text{in}}$.

Proof. Let $(x, v) \in S_{\text{out}}$, then under the flow of (3) we see linear motion. Ignoring the presence of S, we see that depending on v, the trajectory is either periodic or is dense in $\mathbb{T}$.

Focusing on the first case, in finite time we return to the point x. Since the trajectory is a line ℓ interesecting ∂S transversally, there must be another point of intersection $x \neq y \in \partial S \cap \ell$. The velocity at y must also be v, so due to the geometry of a circle, $(y, v) \in S_{\text{in}}$. For the second case, we can pick $\varepsilon > 0$ such that all points in $U = (\partial S \cap B_\varepsilon(x)) \times \{v\} \subset S_{\text{out}}$ are transversal to ∂S. Let

$(y, v) \in U$, since the flow is dense for the velocity v, ignoring S, we know that in finite time the point (x, v) comes to (y, v). The rest of this case follows the same way as previously.

In either case, the (y, v) we find is not necessarily the first time we enter S_{in} but since the number of such points is countable, we can pick the first one (y_0, v), hence, $P_{\text{oi}}(x, v) = (y_0, v)$ is a well-defined map. ■

Now, we can finalize the Poincaré map.

Proposition 2. The sets S_{in} and S_{out} are Poincaré sections with Poincaré maps $P_{\text{in}} = P_{\text{oi}} \circ P_{\text{io}}$ and $P_{\text{out}} = P_{\text{io}} \circ P_{\text{oi}}$, respectively.

Notice that the reasoning is independent of the radius of S, nor does it depend on the exact position of S. Pulling back to the plane with an infinite number of disks, we can then generalize the setup. Consider a fundamental finite set A of disks where each disk in A can have a different magnetic strength and radius and the disks need not be regularly placed. The above result holds for configurations of disks which can be decomposed as a tiling of such a set A.

In [KS17] a similar result is proved for a configuration of finitely many bumps. In that case a different method was used that did not rely on an infinite number of bumps, in ours the reasoning was simplified due to this.

With the Poincaré map we can study the stability of (quasi)-periodic trajectories of the system for a choice of parameters. In fig. 3 we provide some examples we constructed using analytic geometry. In fig. 3a we see a periodic trajectory and its corresponding orbit in the Poincaré section. In fig. 3b we shift the initial condition slightly and see that the orbit in fig. 3a displays stable behavior. We provide a proof using symbolic algebra in HERE. The same can be said comparing fig. 3c and fig. 3d. On the other hand, in add plots with unstable periodic orbit we have a periodic trajectory that does not seem to be stable.

Constructing periodic trajectories and judging their stability by checking numerically is a reliable approach, however it is limited, since we need a good guess to start with. Uncovering more elaborate (quasi)-periodic behavior in this manner becomes impractical, so we need a tool that can help us single out good candidates ahead of time. We discuss this in the next section.

4 Lempel-Ziv and Symbolic dynamics

4.1 Difficulties with symbolic dynamics

In the previous section we discretized the continuous time system via a Poincaré map, and studied some examples of (quasi)-periodic orbits directly. To study the discrete system further, a typical approach taken is to construct a Markov partition, and to pass to a symbol space with a shift map. Providing a Markov partition in our case proved more complicated than expected. We need a better understanding of the (un)stable manifold of a point $x \in S_{\text{out}}$. Furthermore, it is not exactly clear how to "carve" up S_{out} in the first place.

To avoid this, we decided to introduce the Lempel-Ziv complexity as described in [LZ76]. The Lempel-Ziv complexity operates on finite length sequences of symbols by applying a compression algorithm, the complexity of the

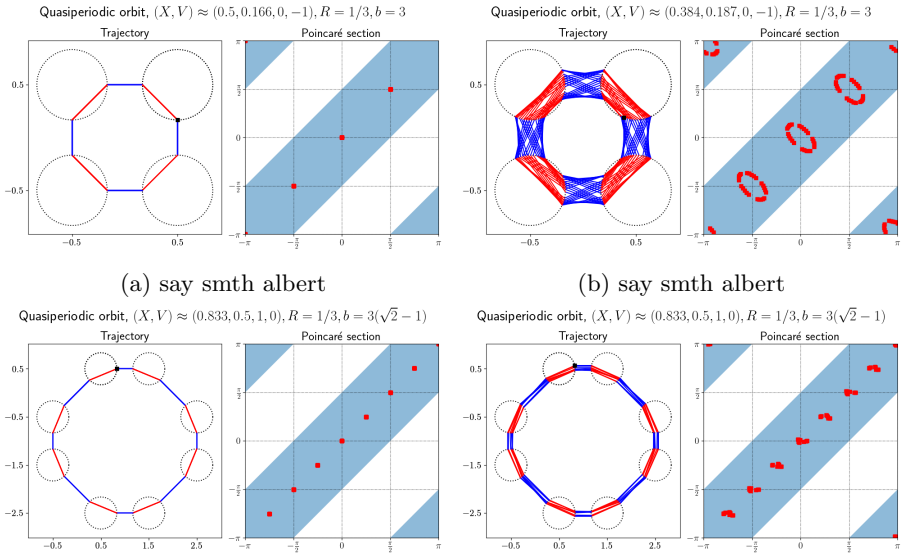

(a) say smth albert

(b) say smth albert

(c) a.

(d) .

Figure 3: Examples of periodic, quasiperiodic, and aperiodic trajectories for varying choices of parameters.

original sequence is then quantified by the result of the compression. Partitioning S_{out} and prescribing an alphabet is still an issue but we first discuss Lempel-Ziv.

4.2 The Lempel-Ziv compression algorithm

To explain the algorithm, we use a series of examples, as in the paper [KS87]. We are not interested in the technicalities of the original paper by Lempel and Ziv, so we only cite results when needed.

Consider a sequence $s = s_1 s_2 \dots s_n$ of length $n \in \mathbb{N}$, the algorithm decides what is the smallest number of "words" in the sequence necessary for reconstruction. Suppose we have reconstructed s up to the index $k < n$ and the word counter is c, that is, we have $s_1 \dots s_k$. For the next iteration, the algorithm decides what is the largest $k < \ell \leq n$ such that the subsequence $s_{k+1} \dots s_\ell$ appears at some index in $s_1 \dots s_{\ell-1}$. Once this ℓ is found, the word counter is increased to $c+1$. If $\ell = n$, then the algorithm terminates, otherwise the process is repeated with $s_1 \dots s_{\ell+1}$. We provide an example below. The $\cdot$ is used as a delimiter between words, the top line indicates the longest subsequence found at each iteration, and the bottom line shows where they can be found.

$$
\begin{aligned}
\overline{0}10110100011011100 10 &\xrightarrow{(1)} 0 \cdot \overline{1}0110100011011100 10 \\
&\xrightarrow{(2)} \underline{0 \cdot 1} \cdot \overline{01}10100011011100 10 \\
&\xrightarrow{(3)} \underline{0 \cdot 1 \cdot 0}11 \cdot \overline{010}0011011100 10 \\
&\xrightarrow{(4)} 0 \cdot 1 \cdot \underline{011 \cdot 01}00 \cdot \overline{01101}110010 \\
&\xrightarrow{(5)} 0 \cdot 1 \cdot 011 \cdot 0\underline{100} \cdot 011011 \cdot \overline{100}10 \\
&\xrightarrow{(6)} \underline{0} \cdot 1 \cdot 011 \cdot 0100 \cdot 011011 \cdot 1001 \cdot \overline{0} \\
&\xrightarrow{(7)} 0 \cdot 1 \cdot 011 \cdot 0100 \cdot 011011 \cdot 1001 \cdot 0
\end{aligned}
$$

At the start, we scan from the left, and notice we have never encountered a 0, so for step (1) we add 0 on its own. Next, we encounter 1 for the first time, and add it in step (2). Next, we see that we have encountered 01, so we add 011. Notice, how we ignore the delimiter between words. We indicate the rest of the steps without commentary. Once the algorithm terminates, we see that the number of words is 7, so the complexity of this sequence is 7.

The complexity is not normalized to $[0, 1]$, this is not needed since we only ever consider finite length sequences and those clearly have bounded LZ complexity. Comparing two sequences of varying length, the sequences can have the same complexity, though it is expected that the longer sequence will have a higher complexity. Now, that we have an idea how the Lempel-Ziv (LZ) complexity is computed, we can discuss how LZ captures the regularity (or lack of it) in symbolic dynamics.

Suppose for now, we have a map taking orbits of a system to elements of a symbol space, then we can distinguish three levels for LZ complexity: high, low, and intermediate. Since LZ is not normalized, and varies depending on the length of the sequences we consider, it is best to work with sequences of the same length. Furthermore, provided we fix the length, the boundary between cases is not well defined. A rule of thumb is to judge the level by comparison, for each system there will be an average complexity for a sampling of orbits, so low complexity will be well below the average and high will be well above. The average can be skewed depending on the sampling but this should be discussed on a case by case basis.

We can characterize the orbits by their complexity as follows:

- If a sequence has high complexity that means we cannot reconstruct the sequence from a small number of words. A word corresponds to some substructure in the orbit, and if there are many unique substructures, we should expect the orbit to be disorganised or chaotic.

- If the complexity is low, meaning very few words are required to reconstruct the sequence, then the corresponding orbit should be regular and repetitive. So, we would expect a (quasi)-periodic orbit to have a low complexity.

- For intermediate complexity the scenario can be mixed. The orbit can appear mostly random with intermitent sections of structure. The orbit can also be (quasi)-periodic but with a significantly longer period for recurrence than an orbit with low complexity.

Of course, this in not formal reasoning and just an intuitive approach. An example where our reasoning breaks down is if a periodic orbit requires n symbols to describe one period and we only sampled n symbols. In this case the complexity can look high, instead of low as one would expect from a periodic orbit. In practice, we find it easy to work around these limitations as will be shown in the next section.

4.3 Partitioning the Poincaré section and compression

Now, to utilize LZ we need a map from orbits to symbol sequences. We have many options here from the partitioning of the Poincaré section to the size of the alphabet, and we do not necessarily need to use a Markov partition for LZ to give us good results. We decided to use a relaxed approach.

Consider the system in the plane, now via the pullback from the torus, S_{out} becomes the outward-pointing boundary of circles centered at lattice points. We know by lemma 2 that a point $x \in S_{\text{out}}$ is mapped to another point on ∂S. We disregard the exact point and velocity of $P_{\text{oi}}(x)$ and only record the relative position of the new circle we intersected. For example, if we have initially $x, v = (1/2, 5/6, 0, 1)$, so we are on the circle centered at $(1/2, 1/2)$, then $P_{\text{oi}}(x, v) = (1/2, 7/6, 0, 1)$ which is on the circle centered at $(1/2, 3/2)$, the symbol we record here is $(1/2, 3/2) - (1/2, 1/2) = (0, 1)$. We see immediately there are infinitely many such pairs $(n, m) \in \mathbb{Z}^2$ that we can attain. We argue that this is not a problem for computing LZ, since there can only be finitely many of these pairs in a finite sequence anyway, i.e, the complexity of a sequence is capped by its length. Another way to look at it: the pairs $(n, m) \in \mathbb{Z}^2$ are words constructed using a finite alphabet $i \in \mathbb{Z}$ with $|i| \leq 9$, so we can unpair the coordinates and work with a stream of integers.

An example to get the idea. Consider the orbit in fig. 3a, the orbit goes down, left, up, right, and repeats, so in symbols that is

$$((0, -1), (-1, 0), (0, 1), (1, 0), \dots),$$

and this pattern repeats indefinitely. To compute LZ, we take a finite slice, for example the first 20 symbols. If computed correctly, LZ should be 5, we record the first 4 symbols as words, and the 5th word is the rest of the 16 symbols, since they just repeat the first 4. The complexity in fig. 3b is also 5, though in fig. 3c and fig. 3d the complexity is 9. We notice also that if we took the first 100 symbols of these orbits, the complexity would still be 5 and 9, respectively, provided they are stable (quasi)-periodic orbits.

4.4 Examples and thoughts

We now look at some examples. We find LZ performs well when we compute it for a range of initial conditions and parameters.

Consider again the examples from fig. 3a and fig. 3b, the second one was obtained by slightly perturbing the initial position and this hints that the periodic trajectory is stable. We ask now how much can we perturb the initial conditions before we leave the region of stability for this periodic orbit. We take $R = 1/3, b = 3$ and compute LZ for the family of intial conditions:

$$x = \left(\frac{1}{2} + \sqrt{R^2 - y^2}, \delta\right), \quad v = (1, 0), \qquad \text{for } y \in [-0.32, 0.32] + \frac{1}{2},$$

that is, we keep the velocity the same, and we sweep the right half-circle centered at $(1/2, 1/2)$. We report the results in fig. 4a. We see that the region of spans values of y roughly in $[0.346, 0.653]$. We also notice there are some dips outside the region of stability. Out of curiosity we plot the orbit of the far left dip in fig. 5a, interestingly, the orbit at first is scattered and then gets trapped between four bumps. Later, we computed more iterations of the orbit and noticed it eventually leaves the four bumps, so it seems the orbit came close to the stable region but did not enter it.

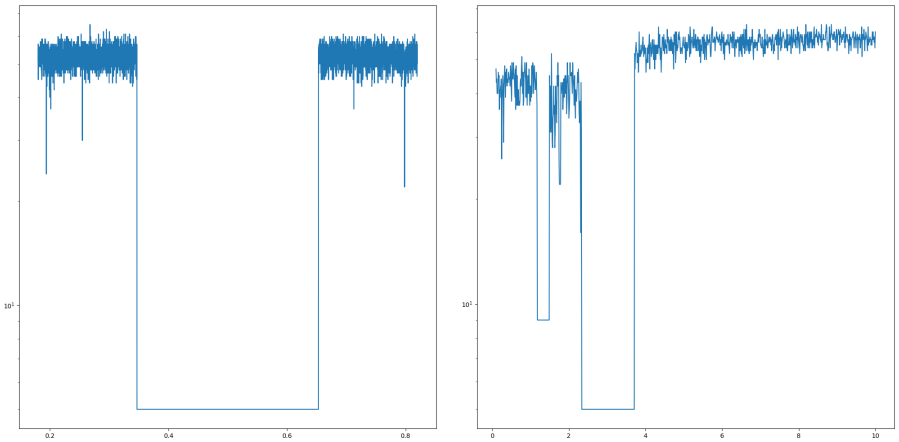

(a) (b)

Figure 4

blabla

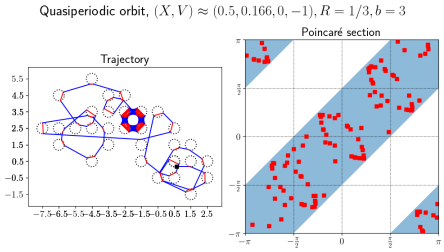

(a) (b)

Figure 5

5 Levy Flights

6 Conclusion

6.1 Further questions

	$b \ll 1$	$b \approx 1$	$b \gg 1$
Uniform perturbation in a disk	Circle Maps	test cases (difficult in general)	Perturbation of Sinai Billiards (maybe)
Arbitrary perturbations	Usual KAM	use paper by Donnay-Liverani	Hard?

Table 1: What it is that we want to do

References

[Coo93] I. D. Coope. Circle fitting by linear and nonlinear least squares. *Journal of Optimization Theory and Applications*, 76:381–388, Feb 1993. https://doi.org/10.1007/BF00939613.

[Eva98] Lawrence C. Evans. *Partial Differential Equations*. American Mathematics Society, 1998. Providence, RI.

[Gas21] Sean Gasiorek. On the dynamics of inverse magnetic billiards. *Nonlinearity*, 34(3):1503–1524, mar 2021. https://doi.org/10.1088%2F1361-6544%2Fabe2f1.

[Kna18] Andreas Knauf. *Mathematical Physics: Classical Mechanics*. Springer Berlin, Heidelberg, mar 2018. https://doi.org/10.1007/978-3-662-55774-7.

[KS87] Kaspar and Schuster. Easily calculable measure for the complexity of spatiotemporal patterns. *Physical review. A, General physics*, 36 2:842–848, 1987.

[KS17] Andreas Knauf and Marcello Seri. Symbolic dynamics of magnetic bumps. *Regular and Chaotic Dynamics*, 22(4):448–454, jul 2017. https://doi.org/10.1134%2Fs1560354717040074.

[LZ76] A. Lempel and J. Ziv. On the complexity of finite sequences. *IEEE Transactions on Information Theory*, 22(1):75–81, January 1976.

[Pö82] Jürgen Pöschel. Integrability of hamiltonian systems on cantor sets. *Communications on Pure and Applied Mathematics*, 35(5):653–696, 1982. https://onlinelibrary.wiley.com/doi/abs/10.1002/cpa.3160350504.

[Ser22] Marcello Seri. *Hamiltonian Mechanics*. AMS Open Math Notes, mar 2022. https://www.ams.org/open-math-notes/omn-view-listing?listingId=110861.